ELSEVIER

Sensors and Actuators A 2997 (2001) 1–7

SENSORS AND ACTUATORS A PHYSICAL

www.elsevier.nl/locate/sna

Microfabrication of a high pressure bipropellant rocket engine

A.P. London[a,*], A.A. Ayón[b], A.H. Epstein[b], S.M. Spearing[a], T. Harrison[a], Y. Peles[a], J.L. Kerrebrock[a]

[a]MIT Gas Turbine Laboratory, Massachusetts Institute of Technology, Cambridge, MA 02139, USA
[b]MIT Microsystems Technology Laboratories, Massachusetts Institute of Technology, Cambridge, MA 02139, USA

Abstract

A high pressure bipropellant rocket engine has been successfully micromanufactured by fusion bonding a stack of six individually etched single crystal silicon wafers. In order to test the device, an innovative packaging technique was developed to deliver liquid coolant and gaseous propellants to the rocket chip at pressures in excess of 200 atm at temperatures above 300°C. Testing continues on the 1.2 g devices, which have been run to date at a chamber pressure of 12 atm, generating 1 N of thrust, and delivering a thrust power of 750 W.
© 2001 Published by Elsevier Science B.V.

Keywords: Rocket; Deep reactive ion etching; MEMS; Combustion; High pressure fluid packaging

1. Introduction

This paper reports the modeling, microfabrication, packaging and initial test results of a first of its kind liquid cooled silicon rocket engine designed to produce 15 N of thrust at a specific impulse of ~300 s. Expected applications include its use on future generations of spacecraft including microsatellites and very small launch vehicles. The later could be used for a number of functions, including deploying large arrays of space probes for tactical, commercial, or scientific applications, and servicing existing satellites [1]. The effort described herein falls within the scope of a larger project currently underway at MIT to develop microheat engines [2] for propulsion and electric power applications, utilizing the processing technology normally associated with the microelectronics industry. The feasibility for these structures originates from (i) the existence of high precision micromachining techniques for making the necessary silicon components, and (ii) the advantageous mechanical characteristics of silicon that make it compatible with applications involving high speed rotating microturbomachinery or exposure to relatively high temperatures. Additionally, the benefits in size reduction can be understood in terms of the cube–square scaling law that suggests an increading energy density with decreasing size, or the feasibility of generating macropower from microdevices.

In particular, the structure described herein is fabricated from single crystal silicon substrates using the recently reported deep reactive ion etching (DRIE) capabilities that allow the micromanufacturing of high aspect ratio features with a prescribed precision. All deep silicon engraving was performed in an inductively coupled plasma etcher (ICP) manufactured by Surface Technology Systems, that has been described elsewhere [3], and that utilizes SF_6 for silicon etching and C_4F_8 for sidewall protection during the etch.

The 125 atm design chamber pressure and small scale of the device leads to an unusually high thrust-to-weight ratio (*T*:*W*) of nearly 1000:1, which roughly corresponds to 20 times that of the space shuttle main engine. The first build of the thrust chamber has demonstrated a power density an order of magnitude larger than has been previously reported for silicon microdevices [4]. At full design conditions, the power density is expected to reach 400 W/mm^3, some 200 times the highest value presently reported.

Section 2 describes the modeling and micromanufacturing of these rocket structures, Section 3 covers issues related to packaging, and testing is discussed in Section 4.

2. Modeling and microfabrication

Silicon was selected as the material of fabrication for primarily two reasons. Firstly, there is an extensive experience and knowledge base associated with the techniques available to fabricate microdevices from it. Secondly, the mechanical material properties of silicon are quite favorable for high-stress, high temperature applications. In fact, its strength-to-density ratio, the primary material figure-of-

* Corresponding author. Fax: +1-210-647-6915.

0924-4247/01/$ – see front matter © 2001 Published by Elsevier Science B.V.
PII: S0924-4247(01)00571-4

UNCORRECTED PROOF

merit for these applications is higher than that of the high temperature metal alloys used in jet engine components today [5].

Having settled on silicon, a parameterized model was developed to obtain a rocket design. The model took into consideration several size, performance and materials inputs, including throat dimensions, chamber length and pressure, number of wafer layers, oxidizer-to-fuel ratio (O:F), and maximum allowed wall temperature. Throughout this exercise the expansion ratio of the nozzle was fixed at 15:1, suitable for high pressure operation at sea level.

The design model generated size, performance and cooling outputs, including engine dimensions and mass, critical wall thickness, thrust, mass flow (f), specific impulse (I_{sp}), residence time (τ_{res}), thrust-to-weight ratio (T:W), characteristic exhaust velocity (c^*), the heat flux profile to the wall, total heat load, the maximum bulk temperature and the minimum required width of the cooling passages.

The cooling design was determined by matching the required heat transfer coefficients along the coolant path to the estimated heat fluxes and total heat loads at different points. Additional 2 and 3D finite element analyses (FEA) were carried out to evaluate the structural integrity of the designed device, with 1 GPa as a reference maximum allowable stress [6]. Finally, 2D thermal models were developed to corroborate the 1D cooling passage design. Microfabrication began once the complete design had been completed.

The fabrication used six 4 in., n-type ⟨1 0 0⟩, single crystal silicon wafers, double side polished, with resistivity of 5–20 Ω cm. Initially all wafers were coated with 2 μm of plasma enhanced chemical vapor deposited (PECVD) silane oxide. This deposited film served a dual purpose: it protected the integrity of all surfaces from scratches and contamination, thus, ensuring the bondability of the wafers involved, and it also served as a hard mask during DRIE, either directly or in nested masks arrangements which allowed separate sets of features to be etched to two different depths from a single side of a wafer. Several topographic features were fabricated using this latter approach. A complete account of the design process and trades considered can be found elsewhere [7,18].

The rocket chamber die is 18 mm × 13.5 mm × 3 mm and is made via the aligned fusion bonding of six silicon wafers (see Fig. 1). The fabrication of this device, which requires 18 anisotropic dry etches and employs 10 photolithographic chrome masks, presented many challenges. Among them: (i) the etching of high aspect ratio fuel injectors repeatably and reliably; (ii) the production of cooling channels with sufficiently large fillet radii at the bottom corners of the produced channels to avoid large stress concentration points; and (iii) performing the bonding of all six silicon laminations with an alignment accuracy ≤3 μm between each pair.

Because the combustion gas temperature is nearly twice that of the melting temperature of silicon, an aggressive cooling system is required. For this purpose, internal cooling

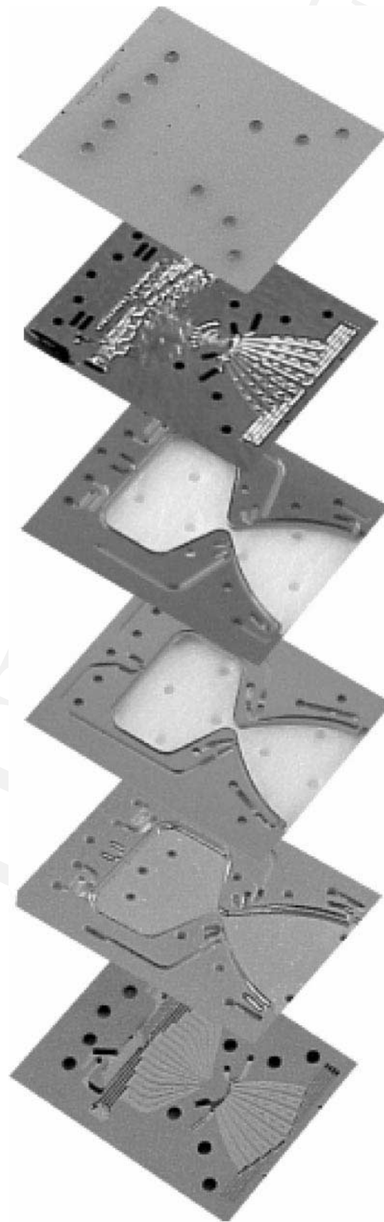

Fig. 1. The six dies from the respective silicon wafers that make up a microrocket stack.

passages are etched in the silicon walls surrounding the combustion chamber. The ethanol coolant flowing through those passages is designed to absorb more than 4 kW of thermal energy at heat fluxes of up to 200 W/mm^2.

In several locations, the design included very narrow features used as cooling passages, adjacent to much wider trenches used as the combustion chamber and exhaust nozzle. In these instances, depth and anisotropy are difficult to control due to the variations in the view angle of the trenches involved as well as the different transport conditions of etchants species and etching byproducts in trenches with large aspect ratio variations. Based on similar layout configurations reported elsewhere [3], the depth of trenches of dissimilar width were made nearly equal by employing

operating conditions with high SF_6 flow rates. Higher flow rates allow for the quick removal of etching byproducts that might otherwise dissociate and redeposit, and provide for the replenishing of etching species, thus, enabling the minimization of the etch depth differential among trenches with unequal exposed areas to plasma etching. The complete set of operating conditions, known as MIT37, is 140 sccm of SF_6 (15 s active etching cycle, 0.5 s of cycle overlap and 12 W electrode power); 95 sccm of C_4F_8 (11 s of active passivating cycle and no electrode power), and with the throttle valve positioned at 65° throughout the process. For those cases, where both depth and surface bottom had to fulfill more stringent requirements, MIT37 was further refined by varying the position of the throttle valve from 65 to 62.5° and by reducing the duration of the passivating cycle from 11 to 9.5 s. The reason for the first modification is that when operating with the throttle or APC valve fixed, the flow rate determines the chamber pressure, thus, lower APC settings produce lower chamber pressures with the concomitant improvement in anisotropy. The justification for the second modification arises from the formation of convex surfaces at the bottom of wide trenches etched with MIT37, situation that is particularly undesirable at the throat of the nozzle. By decreasing the duration of the passivating cycle, the thickness of the protective fluorocarbon film deposited on all surfaces is reduced and the degree of bottom surface convexity was brought within tolerance.

A MIT37 is successful in decreasing depth differential, however, its etching rate is relatively low: ~2 μm/min for an exposed area of 20%, that translates into longer etching times for achieving a prescribed depth. For the same case of narrow and wide trenches located close to each other (within 100 μm), it is possible to control the anisotropy and maintain a higher etching rate, provided the depth differential can be tolerated. This can be accomplished by locating optimum settings for chamber pressure, electrode power [3] and plasma density [8,9]. Generally, anisotropy has a strong dependence on the ratio of electrode power to chamber pressure, thus, lower chamber pressures or higher electrode power operating conditions can help improve anisotropy by increasing the energy of the ions impinging on the wafer surface. However, the same mechanism also lowers the selectivity to masking material, and places a practical limit on the ultimate power/pressure ratio that can be successfully applied. Typical electrode power to chamber pressure ratios are between 200 and 500 mW/mT. Another alternative for trench profile control, is to increase the plasma density, and hence, the ion flux reaching the wafer surface, in order to promote a more efficient removal of the characteristic fluorocarbon films deposited on all surfaces by ICP tools. A practical set of operating conditions can be described as follows: 105 sccm of SF_6 (14 s of active etching cycle, 0.5 s of cycle overlap, 12 W electrode power and 750 W of coil power); 40 sccm of C_4F_8 (11 s of active passivating cycle, no overlap, 6 W electrode power and 600 W of coil power), the throttle or automatic pressure control (APC) valve set at 65°. These etching conditions are known as MIT59 and exhibit a measured etching rate of ~3 μm/min for an exposed area of 20%.

The designed coolant pressure is 300 atm, and highly tailored dry-etching operating conditions are required to produce sufficiently smooth surfaces and large enough feature bottom fillets to withstand the GPa-level stresses created in the walls between the coolant channels and the chamber. There are reports of fillet radii having a strong dependence on chamber pressure [10,11], however, this variable cannot be further modified without compromising the etching characteristics of the operating conditions previously discussed. Instead, and following the recommendations by Chen et al. [12], the process included a 20 s

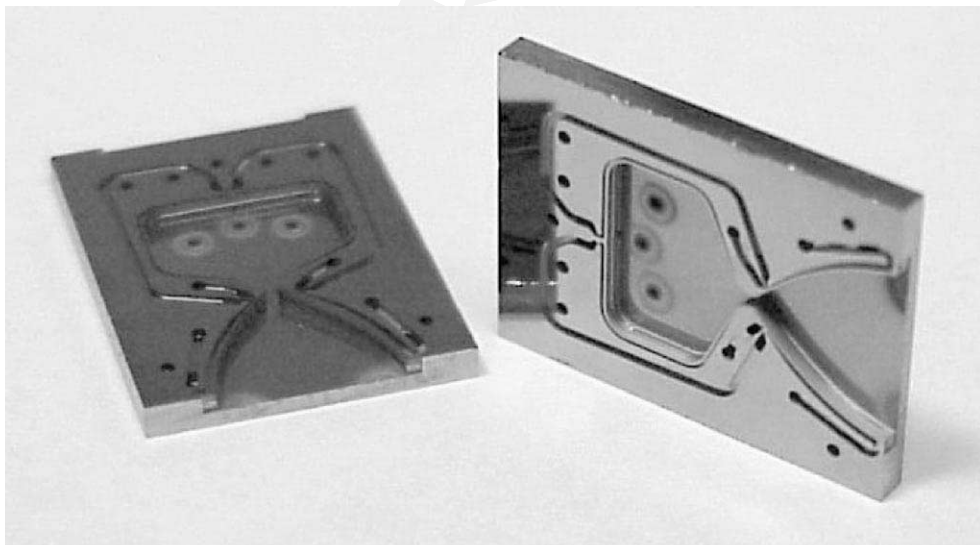

Fig. 2. Two halves of a microrocket thrust chamber. Die size is 18 mm × 13.5 mm × 3 mm.

UNCORRECTED PROOF

Fig. 3. Packaged microrocket die showing the 11 U-shaped stainless steel tubes that connect the silicon chip to the manifold.

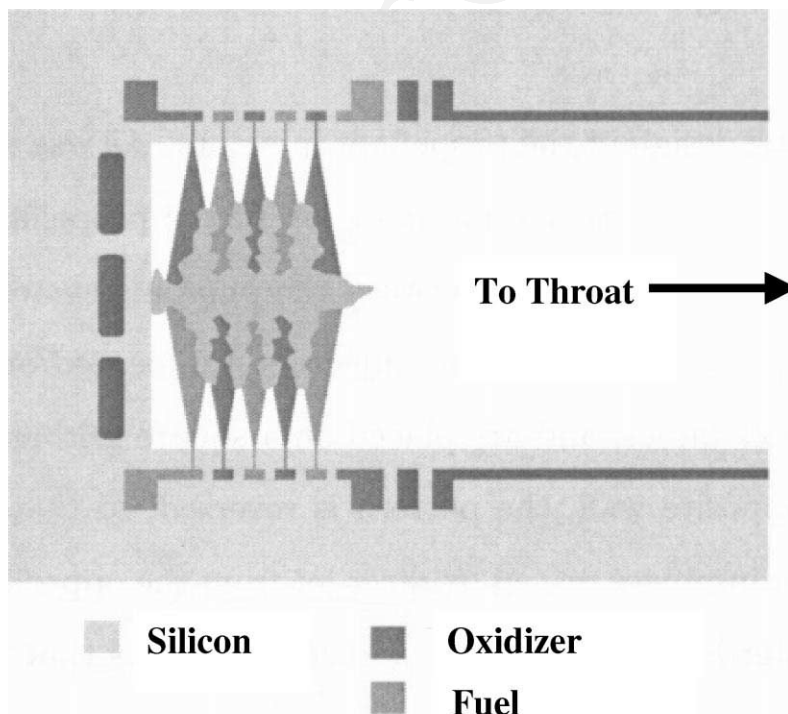

Fig. 4. Each fuel jet shares a centerline axis with, and impinges on, an oxidizer jet from the opposite wall, and vice versa.

UNCORRECTED PROOF

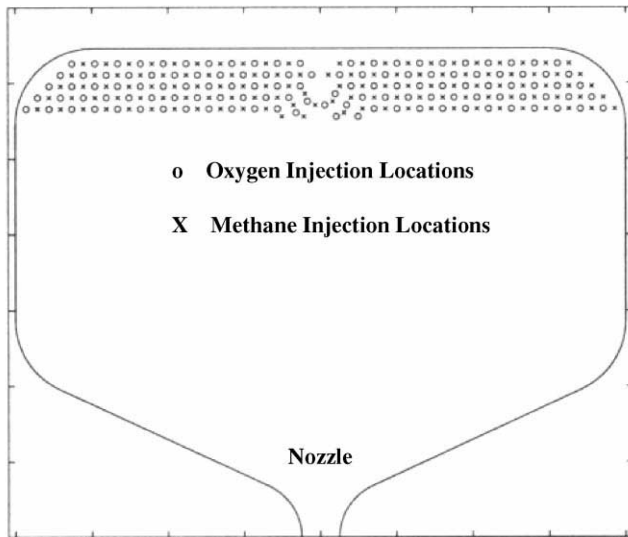

Fig. 5. The injectors are confined to the end of the combustion chamber the farthest away from the nozzle to allow time and distance for the propellants to mix and react.

isotropic etch with an SF_6 plasma after the deep silicon etches, to recover the strength of the etched samples.

Once the six silicon laminations were completed, the remaining protective silicon dioxide films were removed with buffered oxide etch (BOE). The wafers then underwent a standard RCA chemical cleaning procedure [13] to remove organic residues and other contaminants from the silicon surfaces to be bonded, and subsequently all six laminations were aligned and contacted in a single operation that was carried out at room temperature. The six-wafer stack was immediately pressed by applying a pressure on the stack of 60 lb/in.^{2}; the contacting and pressing were performed with equipment from Electronic Visions that has been described elsewhere [14]. Bonding operations are very sensitive to particulates. Specifically, a 1 μm particle can cause the formation of a void with a diameter as large as 1 cm. A subsequent annealing step at 1100°C for 1 h in an inert nitrogen ambient was performed to increase the bond strength of the six-wafer stack [15]. The end result was a monolithic thrust chamber with a mass of 1.2 g (see Fig. 2). Prior to testing, the individual dies were diesawed and packaged.

3. Packaging

An innovative fluidic packaging technique is used (i) to provide for the delivery of the high pressure propellants and coolant to the 11 ports on the rocket chip, and (ii) to tolerate the associated high temperatures during operation [7]. For these purposes, 1 cm long Kovar tubes are glass sealed to the silicon chip, and 10 cm long nickel-plated stainless steel U-

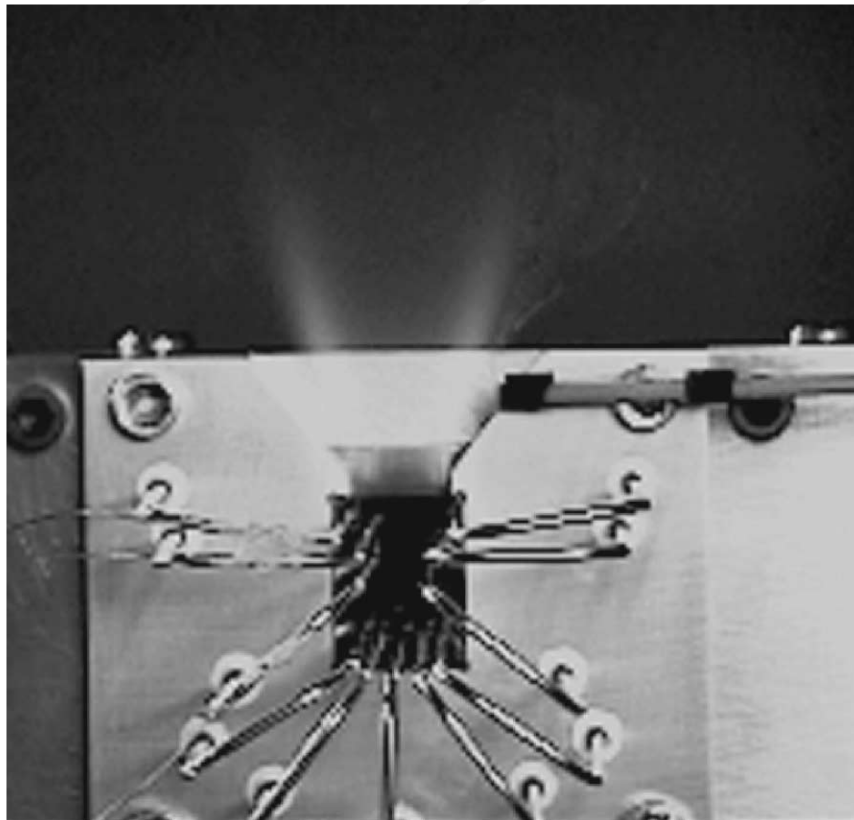

Fig. 6. Visual image of the bipropellant silicon microrocket during operation.

UNCORRECTED PROOF

shaped tubes are used to attach the Kovar tubes to a nickel-plated stainless steel manifold plate using a copper–silver eutectic braze. A glass seal is used for the initial silicon to metal interface because it is feasible to procure glass and metal alloys with coefficients of thermal expansion comparable to that of silicon. Experience has also shown that glass adheres characteristically well to silicon.

The manifold plate is in turn mounted to the macroscale propellant feed system. This feed system and test stand have been designed and constructed to deliver the propellants and coolant at pressures of up to 300 atm to the silicon thrust chamber (see Fig. 3). Additional packaging results can be found elsewhere [16].

4. Testing

The design requires that all wall temperatures remain below 900 K to maintain structural integrity [6]. The original concept for the microrocket engines used liquid oxygen and ethanol as propellants, with both the fuel and oxidizer serving to cool the structure. To simplify the initial testing, the device that has been built was designed to use gaseous oxygen and methane. Ethanol was retained as the coolant, however, as it is an excellent coolant for this application. This is because its critical pressure is only 63 atm, thus, if the coolant pressure can be maintained above this level, the complication of a two-phase flow in the cooling channels can be avoided.

The use of a mixture of oxygen and methane as propellant enables a relatively simple gaseous injection scheme of fuel and oxidizer into the thrust chamber. At the expected operating pressure of 125 atm, and with an oxidizer-to-fuel ratio by mass of 2.3, the predicted chamber temperature is 3150 K.

Due to the dimensions involved in this device, the residence times are inherently small. Additionally, it is known that chemical reaction times do not scale with the size of the reaction vessel [5]. Thus, even though mixing times do scale with size, completion of the combustion, which is necessary for high performance, is a serious concern in devices this small. Recently reported kinetic calculations for a system employing oxygen and ethanol [17], estimate a kinetic reaction time of ~5 μs for a perfectly stirred reactor at a

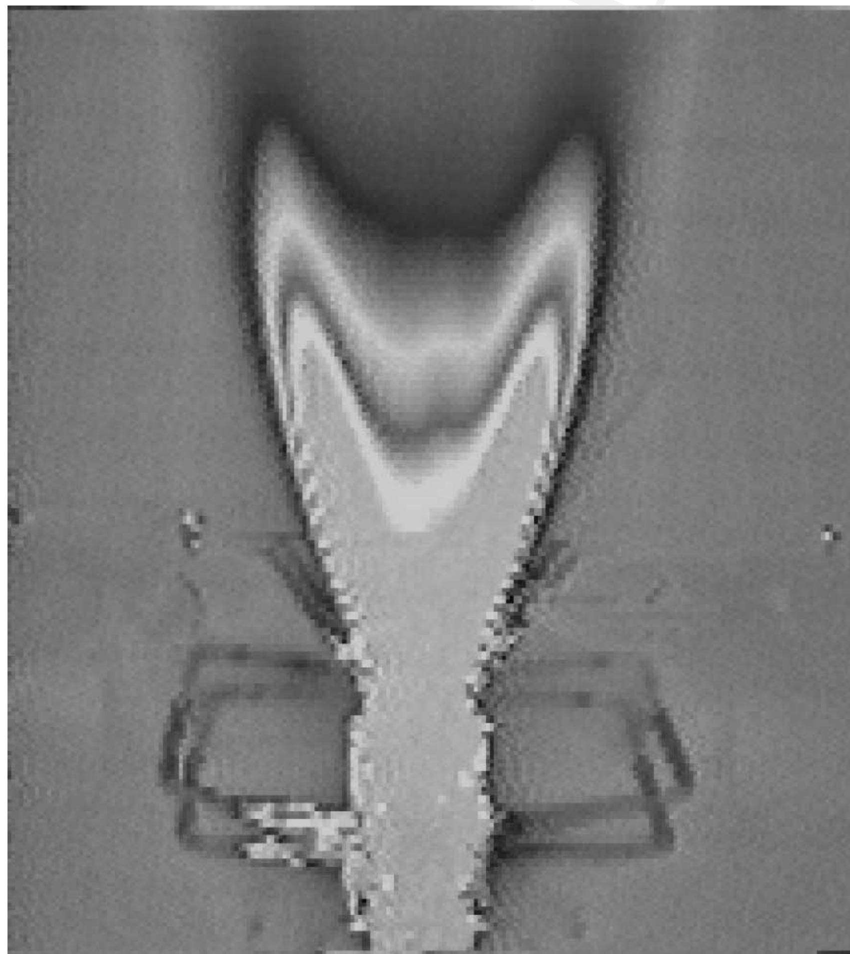

Fig. 7. Infrared image of the bipropellant silicon microrocket operating at 10% of design power.

UNCORRECTED PROOF

pressure of 100 atm. With that value as a reference and in order to provide additional time for mixing and transport of the propellants, the baseline chamber residence time was chosen to be ~100 μs. It is further thought that the mixing time, or time required for diffusion and other transport processes to bring the fuel and oxidizer into sufficiently close proximity for a reaction to occur, can be minimized via a judicious selection of the diameter and spacing of the injector ports. To satisfy these considerations the injectors are located on the upper and lower walls of the combustion chamber, and are placed on a square grid alternating between fuel and oxidizer. On the opposite wall, the pattern is reversed so that each fuel jet shares a centerline axis with, and impinges on, an oxidizer jet from the opposite wall, and vice versa (see Fig. 4). The injectors are confined to the end of the combustion chamber farthest away from the nozzle, in order to allow additional time and distance for the propellants to mix and react as they proceed toward the throat (see Fig. 5). The design includes a total of 484 injectors, 242 each for the oxygen and methane.

The characteristic exhaust velocity, c^*, given by

$$c^* = \frac{P_c A_t}{f}$$

where P_c is the pressure in the combustion chamber, A_t the cross-sectional area of the throat and f the mass flow, is a measure of combustion temperature and effectiveness. For the tests conducted, this velocity appears to be nearly independent of chamber pressure, indicating that chemical reaction rates (which are strongly dependent on pressure) are not limiting the combustion. Additionally, when the effects of chamber heat loss and nozzle separation are included, c^* appears to approach the predicted ideal rocket engine value within 5–15%. This suggests that the transport and mixing of propellants in the combustion chamber is of the right order to provide for complete combustion. Additional performance and other test results can be found elsewhere [7,18].

To date, thrust chambers have been fired five times (see Figs. 6 and 7), achieving chamber pressures of up to 12 atm. Performance at these levels matches predictions to within 5–15%. Testing is continuing with the goal of approaching the design values of 15 N thrust at 125 atm chamber pressure.

5. Conclusions

A rocket engine thrust chamber with a mass of 1.2 g has been fabricated from a stack of six silicon wafers and successfully test-fired. The measured thrust of 1 N yields a useful thrust power of 750 W, and a demonstrated thrust-to-weight ratio for the device of 85:1. At design pressure and with a full expansion in the nozzle, this ratio is expected to be greater than 1000:1, with a thrust power in excess of 20 kW, and a specific impluse approaching 300 s.

Acknowledgements

This work was supported by the NASA Glenn Research Center, Mr. Steven Schneider technical monitor. The cooperation of Dr. Martin Schmidt as well as the staff of the Microsystems Technology Laboratories at MIT is deeply appreciated.

References

[1] T. Beardsley, Fly me to the stars, Sci. Am. (1999) 46.

[2] A. Epstein, S.D. Senturia, G. Anathasuresh, et al., Power MEMS and microengines, in: Proceedings of the 10th International Conference on Solid-State Sensors and Actuators (Transducers'97), Technical Digest, Chicago, IL, USA, 16–19 June 1997, pp. 753–756.

[3] A.A. Ayón, R. Braff, C.C. Lin, H.H. Sawin, M. Schmidt, Characterization of a time multiplexed inductively coupled plasma etcher, J. Electrochem. Soc. 146 (1999) 339–349.

[4] A. Mehra, A.A. Ayón, I. Waitz, M.A. Schmidt, Microfabrication of high temperature silicon devices using wafer bonding and deep reactive ion etching, J. Microelectromechan. Syst. 8 (1999) 152–160.

[5] A.H. Epstein, S.D. Senturia, Science 276 (1997) 1211.

[6] K.-S. Chen, Materials characterization and structural design of ceramic microturbomachinery, Ph.D. Thesis, Massachusetts Institute of Technology, Cambridge, MA, USA, 1999.

[7] A.P. London, Development and test of a microfabricated bipropellant rocket engine, Ph.D. Thesis, Massachusetts Institute of Technology, Cambridge, MA, USA, 2000.

[8] A.A. Ayón, R.A. Braff, R. Bayt, H.H. Sawin, M.A. Schmidt, Influence of coil power in the etching characteristics in a high density plasma etcher, J. Electrochem. Soc. 146 (1999) 2730–2736.

[9] A.A. Ayón, X. Zhang, R. Khanna, Ultra deep anisotropic silicon trenches using deep reactive ion etching (DRIE), in: Proceedings of the 2000 Solid State Sensors and Actuator Workshop, Technical Digest, Hilton Head, SC, USA, 5–8 June 2000, pp. 339–342.

[10] K.-S. Chen, A.A. Ayón, K.A. Lohner, M.A. Kepets, T.K. Melconian, S.M. Spearing, Dependence of silicon fracture strength and surface morphology on deep reactive ion etching conditions, in: Proceedings of the Symposium Fall Meeting of the Materials Research Society, Vol. 546, Boston, MA, USA, 30 November–4 December 1999, pp. 21–26.

[11] A.A. Ayón, K. Ishihara, R. Braff, H.H. Sawin, M. Schmidt, Deep reactive ion etching of silicon, in: Proceedings of the Symposium Fall Meeting of the Materials Research Society, Vol. 546, Boston, MA, USA, 30 November–4 December 1999, pp. 51–61.

[12] K.-S. Chen, A. Ayón, S.M. Spearing, Controlling and testing the fracture strength of silicon on the mesoscale, J. Am. Ceram. Soc. 83 (2000) 1476–1484.

[13] W. Kern, The evolution of silicon wafer cleaning technology, J. Electrochem. Soc. 137 (1990) 1887–1891.

[14] A.R. Mirza, A.A. Ayón, Silicon wafer bonding for MEMS manufacturing, Solid State Technol. 42 (1999) 73–78.

[15] Q.-Y. Tong, U. Gösele, Semiconductor Wafer Bonding, Wiley, New York, 1999, pp. 106–122.

[16] T. Harrison, M.S. Thesis, Massachusetts Institute of Technology, Cambridge, MA, USA, 2000.

[17] O. Al-Midani, Preliminary design of a liquid bipropellant micorfabricated rocket engine, M.S. Thesis, Massachusetts Institute of Technology, Cambridge, MA, USA, 1998.

[18] A.L. London, A.H. Epstein, J.L. Kerrebrock, A high pressure bipropellant microrocket engine, in: Proceedings of the AIAA Joint Propulsion Conference, Huntsville, AL, USA, 2000, AIAA, 2000, p. 3164.

UNCORRECTED PROOF